

Long-Range Optical Wireless Information and Power Transfer

Yunfeng Bai, Qingqing Zhang, Wei Wang, Riqing Chen and Qingwen Liu, *Senior Member, IEEE,*

Abstract

Simultaneous wireless information and power transfer (SWIPT) is a remarkable technology to support data and energy transfer in the era of Internet of Things (IoT). In this paper, we propose a beam-compression resonant beam (BCRB) system for long-range optical wireless information and power transfer based on the telescope-like internal modulator (TIM). Utilizing the TIM, the resonant beam is compressed, making the transmission energy be further concentrated. Thus the over-the-air power loss produced by the beam diverged decreases, which enables the long-range SWIPT capability. We establish the analytical models of the transmission loss, the stability condition, the output power, and the spectral efficiency of the BCRB system, and evaluate the performance on the beam-compression, energy delivery, and data transfer. Numerical analysis illustrates that the exemplary BCRB system can deliver 6 W power and have 14 bit/s/Hz spectral efficiency over 200 m distance. Overall, the BCRB system is a potential scheme for long-range SWIPT in IoT.

Index Terms

Optical beams, Telescopes, Energy conversion, Optical communication, Optical diffraction

Y. Bai, and Q. Liu, are with the College of Electronic and Information Engineering, Tongji University, Shanghai, 201804, China, (email: baiyf@tongji.edu.cn, qliu@tongji.edu.cn).

Riqing Chen is with the Digital Fujian Institute of Big Data for Agriculture and Forestry, Fujian Agriculture and Forestry University, Fuzhou, P.R. China. (e-mail: riqing.chen@fafu.edu.cn).

W. Wang is with the Shanghai Institute of Optics and Fine Mechanics, Chinese Academy of Sciences, Shanghai, China. (email: wangwei2016@siom.ac.cn).

Qingqing Zhang is with the School of Electronic Information and Communications, Huazhong University of Science and Technology, Wuhan 430074, China (e-mail: q_zhang@hust.edu.cn).

I. INTRODUCTION

With the rapid growth of the Internet of Things (IoT), countless network devices are interconnected in various scenarios for making our life smart and convenient. However, since the applications are becoming more complex, their demands for communication capacity and energy supply increase dramatically [1]–[5]. Therefore, simultaneous wireless information and power transfer (SWIPT) technology has recently attracted wide attention to providing both information and energy at the same time [6]. SWIPT technologies can be classified into two types: wide-area omnidirection and narrow-beam orientation. Wide-area omnidirectional technology such as broadcasting radio-wave can support long-distance and omnidirectional SWIPT [7]. However, the broadcasting energy emission results in energy dissipation, which is difficult to achieve high-power transmission. Narrow-beam orientation technology such as beamforming/laser can support high-efficiency transmission [8]. But using the narrow electromagnetic beam always accompanies the challenges of mobility and safety. For instance, Das *et al.* in [9] present a receiving device that can harvest sunlight energy and signal light data at the same time. By separating the energy beam from the communication beam, this scheme can realize safe SWIPT. However, it is not mobile and cannot operate under sunless conditions such as night. To meet the requirements of high power, safety, and mobility, the resonant beam system has been proposed [10].

The RB system using the lightwave as the energy and data carrier belongs to the narrow-beam orientation type which can support the high-efficiency transmission with the line of sight (LoS) between the transmitter and the receiver. The transmission of the resonant beam will cease immediately due to object intrusion, which ensures safety. Moreover, at both the transmitter and the receiver, retro-reflective structures are adopted to realize self-alignment mobility [11]. Furthermore, the optical carrier of resonant beam enables the ability of high-rate data transfer due to huge available bandwidth and high signal-to-noise ratio [12]. Fig. 1 depicts the application scenarios of the RB system. Devices such as the unmanned aerial vehicle (UAV), smartphones, laptops, etc., can be supported by it [13].

The idea of the RB system was firstly proposed in [10] and analyzed in [14]. An adaptive RBC (ARBC) system for battery charging optimization [15]. A system has been demonstrated to achieve 2 W power transfer over 2.6 m distance in lab test [16]. An analytical model to depict information transfer in the RB system has been present in [17]. A time-division multiple access (TDMA) method was put forward to support multi-user scenarios [18]. A first-access-

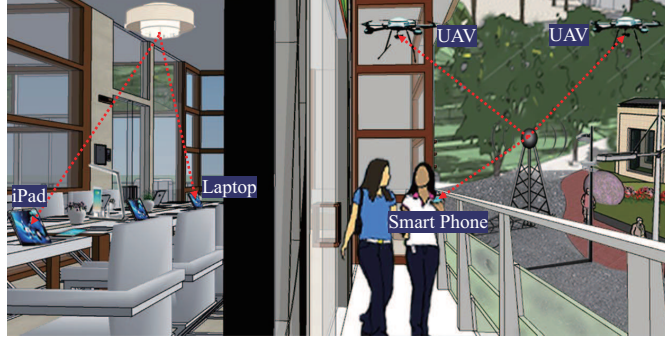


Fig. 1. Resonant Beam Systems Application Scenarios

first-charge (FAFC) scheduling algorithm was proposed to keep all devices working as long as possible for fairness [19]. A design was presented in [11] to demonstrate the mobility of the RB system based on retro-reflectors. An analytical model based on the electromagnetic field was established for assessing the safety of the RB system [20]. The above research works explored the system structures and theoretical principles of RB. However, the transmission performance of the RB system in the literature is only a few meters, which limits its application scenarios such as large warehouses and outdoor spaces. In this paper, we propose a long-range optical wireless information and power transfer system based on the resonant beam and telescope-like internal modulator (TIM). The TIM can compress the resonant beam, reduce the transmission loss, and thus enhance the transmission distance.

The contributions of this paper are as follows:

- A beam-compression resonant beam (BCRB) system scheme based on the telescope-like internal modulator (TIM) is proposed which can restrain the transmission loss and achieve long-range optical wireless information and power transfer.
- An analytical model of the BCRB system is established, which can depict the stable condition, beam distribution, deliverable power, and communication ability.
- We illustrate via numerical analysis that the proposed BCRB system can transfer multi-watt power over several hundred meters with 14 bit/s/Hz spectrum efficiency.

In the rest of this paper, the introduction of the system fundamental principle will be illustrated in Section II. The analytical model of the BCRB system will be developed in Section III. The performance of the BCRB system will be evaluated in Section IV. Finally, conclusions will be made in Section V.

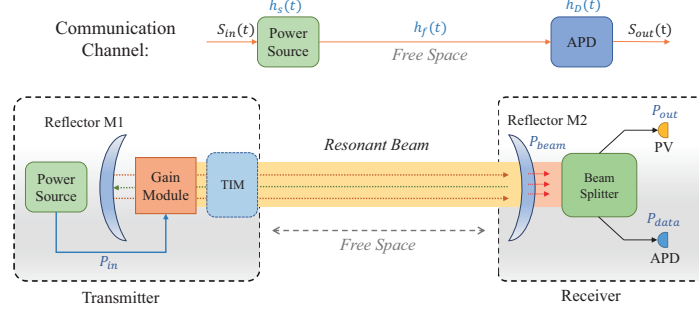


Fig. 2. System Diagram

II. SYSTEM FUNDAMENTAL PRINCIPLE

Figure 2 shows the schematic diagram of the BCRB system. The system consists of the transmitter and the receiver, which are separated in space. The transmitter includes a reflector M1, a power source, a gain module, and a TIM. The receiver includes a reflector M2, a beam splitter, a photovoltaic (PV) cell, and an avalanche photodiode (APD) [21], [22]. Reflectors M1, M2, and gain module form a spatially separated laser resonator (SSLR) cavity, which is used to generate and transmit the resonant beam. These elements are coated with anti-reflection coating to suppress reflection loss. Before establishing the system analytical model, we need to elaborate on the basic principles of system energy penetration, communication, and transmission loss.

A. Energy Conversion

The energy conversion process of the system can be divided into three phases: energy absorbing, stimulated emission, and beam output. 1) *Energy absorbing*: The input electrical power is converted to pump beam power in the power source. Then, with the pump beam radiating to the gain module, the particles in the gain module will be activated, which leads the particles being transited from low energy level to high energy level. Finally, population inversion occurs and energy is stored in the gain module. 2) *Stimulated radiation*: With the pump power input, particles are transited to the high energy level, continuously. Since particles in high energy level are unstable, they will fall back to the lower level with spontaneous and stimulated radiation and emit photons. 3) *Beam output*: These emitted photons will propagate between the reflector M1 and the reflector M2, accompanying the gain and loss. Finally, photons begin oscillating and form the resonant beam.

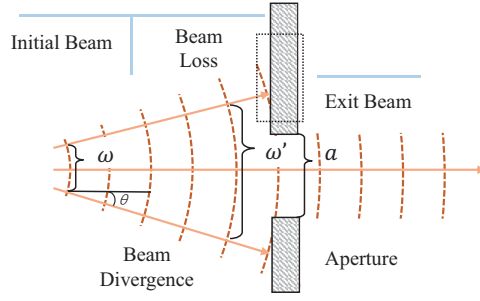


Fig. 3. Transmission Loss

B. Signal Generation

Before the pump beam is radiated to the gain module, its amplitude and phase will be modulated to load the signal. Then the gain module receives the pump beam and generates an excitation beam with the same amplitude and phase as the pump beam making the signal be delivered into the resonant cavity. Finally, the modulated beam transfers through the free space and is received by the APD detector. The communication process of the proposed system is similar to traditional space optical communication, which can be modeled as a linear time-invariant system [23]:

$$s_{out}(t) = h_s(t) * h_f(t) * h_D(t) * \gamma P_{data} s_{in}(t) + n_t(t). \quad (1)$$

Eq. (1) describes the process of signal change from pump source to ADP. γ expresses the APD's responsivity, and $n(t)$ is the additive white gaussian noise (AWGN), and $h_s(t)$, $h_f(t)$, and $h_D(t)$ are the impulse response functions of the adjustable power source, the free space and the APD detector, respectively.

C. Transmission Loss

There are many losses that affect the output performance of the system, such as heat loss, absorption loss, reflection loss, and transmission loss. Among them, transmission loss is associated with the transmission path of the beam and will gain as the transmission distance increase, which greatly impacts the range of the beam transfer. According to [24], the transmission loss comes from the beam diffraction and overflow on the finite aperture, which can be depicted in Fig. 3. The beam propagates in the free space. Since the divergence angle θ existed, beam divergence will generate along with the transmission path, and the beam spot (beam cross-section) becomes

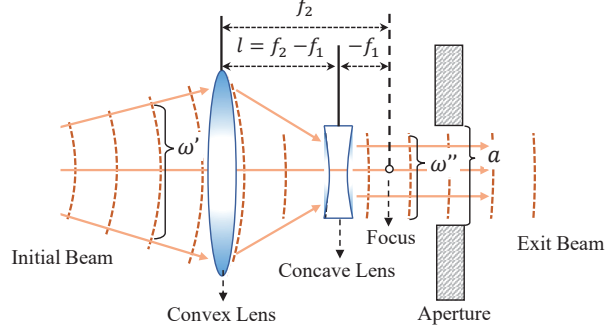


Fig. 4. Beam Compressed by TIM

large, making the spot diameter enlarge from ω to ω' . An aperture exists on the beam path and the diameter of its geometric boundary is a . When the beam passes the aperture, if ω' is bigger than a , some part of the beam will hit on the aperture's boundary, which causes the beam loss either by spillover accompanying the diffraction. Since the beam divergence gain with the distance, the loss will also increase. When the energy loss is large enough over a certain distance, the power output of the system will be stopped. In this process, a large diffraction loss will be produced if beam spot is much larger than the aperture. In contrast, diffraction loss will be small if the beam spot is controllable and most beam can pass the aperture instead of being blocked or overflow [25], [26].

III. ANALYTICAL MODEL FOR BCRB SYSTEM

In this section, we will analyze the TIM first. Then, the stable condition of the BCRB system will be established, and models about the system beam spot, beam power, and communication

TABLE I
MATRIX EXPRESSION

M_{m_1}	M_{m_2}	M_{D_0}	M_{D_1}	M_{D_2}	M_{L_1}	M_{L_2}	M_{L_3}	M_M
$\begin{bmatrix} 1 & 0 \\ -\frac{1}{\rho_1} & 1 \end{bmatrix}$	$\begin{bmatrix} 1 & 0 \\ -\frac{1}{\rho_2} & 1 \end{bmatrix}$	$\begin{bmatrix} 1 & 0 \\ -\frac{1}{f_R} & 1 \end{bmatrix}$	$\begin{bmatrix} 1 & f_1 \\ 0 & 1 \end{bmatrix}$	$\begin{bmatrix} 1 & -f_2 \\ 0 & 1 \end{bmatrix}$	$\begin{bmatrix} 1 & L_1 \\ 0 & 1 \end{bmatrix}$	$\begin{bmatrix} 1 & L_2 \\ 0 & 1 \end{bmatrix}$	$\begin{bmatrix} 1 & L_3 \\ 0 & 1 \end{bmatrix}$	$\begin{bmatrix} M & 0 \\ 0 & \frac{1}{M} \end{bmatrix}$

will be developed. These models lay an analytical foundation for the performance evaluation of the BCRB system in Section IV.

A. Telescope-like Internal Modulator

From the analysis above, we know the fact that beam divergence will cause transmission loss. Thus, if the beam can be compressed before it enters the aperture transmission loss can be restrained. Fig. 4 shows the schematic of the TIM and the process of the beam compression. The TIM is composed by a concave lens and a convex lens, and their focal length is $-f_1$ and f_2 . Two lenses are placed in parallel, and their focuses are overlap [27]. When the resonant beam enters the TIM, it will first pass the convex lens. Under the function of the lens, the phase of the beam is changed, which makes the beam transmit toward the lens's focal point. Then, the beam passes the concave lens, and a second phase change is undergone, which leads the beam parallelly emitting from the concave lens. In general, these phase changes compress and collimate the incident beam, which converts the beam spot diameter from ω' to ω'' . When ω'' is smaller than the aperture diameter a , most of the beam will pass the aperture and the loss is restrained. According to the schematic diagram of the BCRB system presented in Fig. 2. The system consists of a reflector M1, M2, a TIM, and a gain module. In these elements, the smallest aperture which will produce the transmission loss is the gain module [16]. Therefore, the TIM is set on the side of the gain module close to the receiver. When the beam is reflected back from the receiver, the divergent and enlarged beam caused by long-distance transmission will be compressed by the TIM before it enters the gain module. According to the above analysis, the transmission loss of the system is restrained, which will enhance the transmission performance of the system.

B. Stable Condition of Resonant Cavity

To guarantee the cyclic oscillation of the resonant beam, the resonant cavity of the BCRB system needs to satisfy the stable resonant cavity condition since it can restrain photons overflowing when photons propagate between the transmitter and the receiver [26].

1) *Transmission matrix*: To get the stable condition of the BCRB system, the propagation of the beam in the cavity should be depicted at first. We introduce the vector and matrix to accurately and strictly analyze the beam transfer [26]. Fig. 5 shows the process of beam propagation depicted by the transmission matrix. As can be seen, incident beam is expressed as $\vec{r}_1 = (x_1, \theta_1)$, where x_1

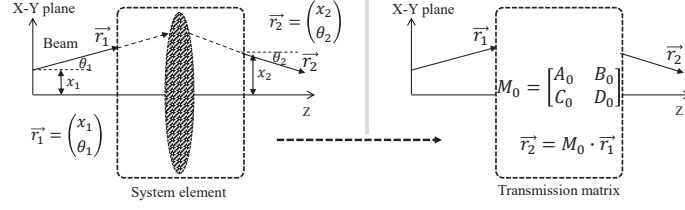


Fig. 5. Beam Propagation Depicted by Transmission Matrix

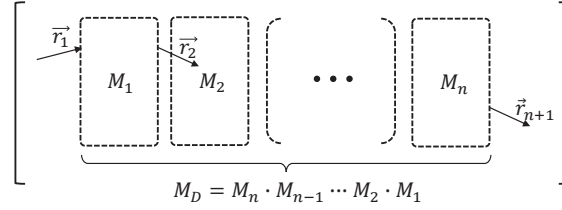


Fig. 6. Beam Propagation in Concatenate Elements

expresses the start point location and θ_1 expresses the inclination angle. After beam propagated through a system element (such as convex lens), the vector \vec{r}_1 converts to $\vec{r}_2 = (x_2, \theta_2)$ with the function of the element. Using transmission matrix M_0 to express the beam propagating through the medium, the conversion process can be defined as

$$\vec{r}_2 = M_0 \vec{r}_1 = \begin{bmatrix} A_0 & B_0 \\ C_0 & D_0 \end{bmatrix} \vec{r}_1, \quad (2)$$

where A_0, B_0, C_0, D_0 are matrix elements determined by the medium structure.

Then, we consider the beam propagating through space with several elements. The process is depicted in Fig. 6. The beam vector \vec{r}_1 starts on the left. After passing the first element, \vec{r}_1 is converted to \vec{r}_2 and so next. If the space has n elements with matrices $M_1 \sim M_n$, \vec{r}_1 is finally converted to \vec{r}_{n+1} and

$$\vec{r}_{n+1} = M_n \cdots M_2 M_1 \vec{r}_1 = M_C \vec{r}_1, \quad (3)$$

where M_C is concatenated by $M_1 \sim M_n$.

2) *Stable condition development*: Since the transmission matrix has been developed, we can describe the beam propagation within the cavity and obtain the stable condition. In the BCRB system, taking the position of beam at M1 as the starting point, the beam will pass through M1,

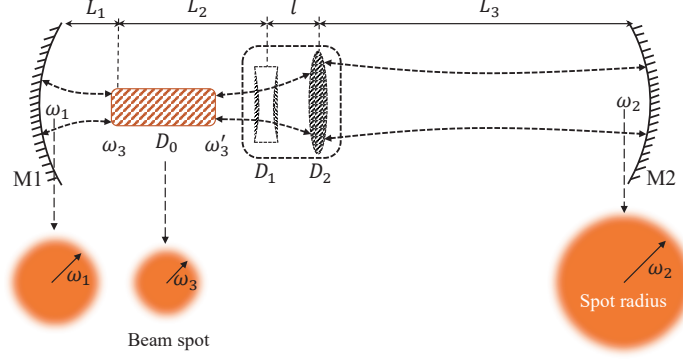


Fig. 7. Parameters Diagram of BCRB System

the gain module, the convex lens and concave lens to M2 in succession. Same as above, the beam propagation can be depicted by transmission matrix as:

$$\begin{aligned}
 M_{C_1} &= M_{m_2} M_{L_3} M_{D_2} M_M M_{D_1} M_{L_2} M_{D_0} M_{L_1} M_{m_1} \\
 &= \begin{bmatrix} 1 & 0 \\ -\frac{1}{\rho_2} & 1 \end{bmatrix} \begin{bmatrix} 1 & L_3 \\ 0 & 1 \end{bmatrix} \begin{bmatrix} 1 & -f_2 \\ 0 & 1 \end{bmatrix} \\
 &\quad \begin{bmatrix} M & 0 \\ 0 & \frac{1}{M} \end{bmatrix} \begin{bmatrix} 1 & f_1 \\ 0 & 1 \end{bmatrix} \begin{bmatrix} 1 & L_2 \\ 0 & 1 \end{bmatrix} \\
 &\quad \begin{bmatrix} 1 & 0 \\ -\frac{1}{f_R} & 1 \end{bmatrix} \begin{bmatrix} 1 & L_1 \\ 0 & 1 \end{bmatrix} \begin{bmatrix} 1 & 0 \\ -\frac{1}{\rho_1} & 1 \end{bmatrix} \\
 &= \begin{bmatrix} A_1 & B_1 \\ C_1 & D_1 \end{bmatrix}, \tag{4}
 \end{aligned}$$

where M_{m_1} , M_{m_2} , M_{D_0} , M_{D_1} , M_{D_2} and M_M represent the transmission sub-matrix of beam propagating through the reflector M1, M2, the gain module D_0 , and the TIM with elements D_1 , D_2 and l . A parameter M which can be depicted as

$$M = \frac{f_2}{f_1} \tag{5}$$

is introduced for defining the TIM structure. Besides, it should be noted that the matrix M_M is converted from M_l through matrix operation, in order to simplify the formula expression and the performance evaluation in Section IV. M_{L_1} , M_{L_2} , and M_{L_3} is introduced to depict the process of the beam passing the free space with different space distance L_1 , L_2 and L_3 .

M_{C_1} is concatenated by $M_{m1}, M_{m2} \sim M_M$, which expresses the single-pass propagation of the beam in the cavity. Based on [28], we herein use a plane mirror and a lens as a combination to replace the end mirror. At this time, M_{C_1} can depict the whole beam propagation inside the cavity. The parameters diagram of BCRB system is shown in Fig. 7, and the specific forms of the transmission sub-matrix are listed in Table I [25], [26], [29]. After matrix calculation, the concrete expression of M_{C_1} can be obtained and the matrix elements of it are

$$M_{C_1} \begin{cases} A_1 = M - \frac{L'_3/M + L'_2 M}{f_R} - \frac{B_1}{\rho_1} \\ B_1 = L_1 \left(M - \frac{L'_3/M + L'_2 M}{f_R} \right) + L'_2 M + \frac{L'_3}{M} \\ C_1 = \frac{A_1 D_1 - 1}{B_1} \\ D_1 = \frac{1}{M} - \frac{L_1}{f_R M} - \frac{B_1}{\rho_2} \end{cases}, \quad (6)$$

where $L'_2 = L_2 + f_1$ and $L'_3 = L_3 - f_2$ are used to make (6) concise. From (6), comparing with the original system, the transmission matrix of BCRB adds three impacts M, f_1 and f_2 brought from TIM. From a mathematical point of view, these parameters make the matrix more flexible and variable. Through designing these parameters, the transmission matrix is adjusted, and the beam propagation can be changed for different demand, correspondingly. According to [30] and symbolic calculation, to keep the beam stably propagating within the cavity, the relationship of the structure parameters from the transmission matrix M_{C_1} :

$$0 < \left(M - \frac{L'_3/M + L'_2 M}{f_R} - \frac{B_1}{\rho_1} \right) \cdot \left(\frac{1}{M} - \frac{L_1}{f_R M} - \frac{B_1}{\rho_2} \right) < 1. \quad (7)$$

Based on (7), substituting fixed boundary parameters and combining control variate, the restriction condition of the characteristic parameter such as the theoretical maximum distance can be determined.

C. Beam Spot Radius

The beam spot is the intensity distribution of the beam in the vertical propagation direction, we can use spot radius to depict the beam spot size. We develop the beam transmission matrix

which can depict the beam propagation in BCRB system, and achieve the stable condition of the BCRB system. Based on it, the beam spot radius on the M1 and M2 can be given by [30]:

$$\begin{aligned}\omega_1^4 &= -\left(\frac{\lambda}{\pi}\right)^2 \frac{B_1^2 D_1}{A_1(A_1 D_1 - 1)}, \\ \omega_2^4 &= -\left(\frac{\lambda}{\pi}\right)^2 \frac{B_1^2 A_1}{D_1(A_1 D_1 - 1)},\end{aligned}\tag{8}$$

where ω_1 and ω_2 represent the beam mode radius on the M1 and M2, respectively; A_1, B_1, C_1 , and D_1 are the matrix elements of M_{C1} ; λ is the wavelength of the resonant beam.

The propagation of the resonant beam in the cavity follows the law of the Gaussian beam [28]. Therefore, taking the beam spot on M1 as reference, after a propagation for a distance L_1 , the expression of beam spot radius on the gain module ω_3 can be defined as

$$\omega_3^2 = \omega_1^2 \left[\left(1 + \frac{L_1}{\rho_1}\right)^2 + \left(\frac{L_1 \lambda}{\pi \omega_1^2}\right)^2 \right],\tag{9}$$

where ρ_1 represents the curvature radius of end reflector. Since L_1 and the length of the gain module are short and far less than the transmission distance d , the beam divergence over this short distance can be negligible. Therefore, ω_3 can be approximately equal to ω_1 and ω'_3 (the beam spot radius on the right border of the gain module), which simplifies the calculation process.

D. External Beam Power

According to Section II, after the processes of energy-absorbing and stimulated radiation, the resonant beam generates and will cyclically oscillate in the cavity. Part of the beam will emission from the reflector M2 as a function of the external beam. Based on the cyclic power principle, the external beam power can be expressed as [25]:

$$P_{beam} = \frac{2(1-R)\eta_c}{(1+R)(\delta_t - \ln R)} P_{in} + C,\tag{10}$$

TABLE II
SYMBOLS EXPRESSION

Symbol	Expression
ρ_1, ρ_2	Curvature radius of $M1, M2$
f_R, f_1, f_2	Focal length of D_0, D_1, D_2
L_1, L_2, L_3	Distance between $M1$ and D_0 , D_0 and D_1 , D_2 and $M2$

where R is the effective reflectivity compounded by R_2 and constant energy loss. η_t expresses the compounded energy conversion efficiency which is determined by the overlap, stored energy efficiency. C is the intercept power. δ_c is the compounded transmission loss. Since the space loss coming from the air compounded is neglected, the transmission loss can be defined as [16]:

$$\delta_t(d) = N e^{-2\pi \frac{b^2}{\lambda d}}, \quad (11)$$

where N expresses the scale factor of the model, d expresses the distance between the transmitter and the receiver corresponding to L_3 in Fig. 7, and b expresses the radius of finite aperture inside the cavity which is the geometric boundary of the gain module in RB system. Due to the function of TIM, the resonate beam is compressed before it enters the gain module, the transmission loss produced on the gain module be greatly reduced or negligible to a certain extent. At this time, the loss will be produced from the TIM, since it also has a geometric boundary. However, compared with the gain module, the geometric boundary of the TIM is adjustable and large.

E. Energy Harvesting and Data Receiving

To achieve information and energy transfer simultaneously, the external beam power is split by a beam splitter. One stream is for energy harvesting and the other is for data receiving.

1) *Energy harvesting*: External beam propagates to the PV cell through the optical waveguide and will be converted to electrical power by photoelectric conversion. The process can be defined as [15]:

$$P_{out} = a_1 \mu P_{beam} + b_1, \quad (12)$$

where a_1 and b_1 are the inherent parameters of the PV cell, and μ is the split ratio.

2) *Data Receiving*: Avalanche photodiode (APD) receives the optical signal carried by the external beam and converts it into an electrical signal. This process can be expressed as

$$P_{data} = \gamma(1 - \mu)P_{beam}, \quad (13)$$

where γ is the parameter of the optical-to-electrical conversion responsivity of APD. In the process of photoelectric conversion, the thermal noise and shot noise will generate. Firstly, the shot noise can be defined as [31]:

$$n_{shot}^2 = 2q(P_{data} + I_{bg})B_x, \quad (14)$$

where q is the electron charge, B_x is the bandwidth, I_{bg} is the background current. Then the thermal noise is [31]:

$$n_{thermal}^2 = \frac{4KT B_x}{R_L}, \quad (15)$$

where K is the Boltzmann constant, T is the background temperature, and R_L is the load resistor. Furthermore, we can depict the significant AWGN noises, which is

$$n_{total}^2 = n_{shot}^2 + n_{thermal}^2. \quad (16)$$

Finally, the spectral efficiency of the BCRB system can be described as [32]:

$$\tilde{C} = \frac{1}{2} \log\left(1 + \frac{P_{data}^2 e}{2\pi n_{total}^2}\right). \quad (17)$$

IV. NUMERICAL EVALUATION

In the section above, a BCRB system scheme based on the TIM is proposed, and the analytical model of the system is developed. In this section, to evaluate the transmission performance of the BCRB system, we will compare the transmission and output power performance between the original and BCRB systems at first. Then, we will analyze the impact of structure parameters on the transmission distance, beam-compression capabilities, output power, data receiving, giving the achievable performance of the BCRB system.

A. Performance Comparison

BCRB system has a built-in TIM, which can compress the incident beam and improve the transmission performance. To verify this point, we will compare the beam distribution, transmission distance, and the output beam power of the proposed system with the original system.

1) *Beam spot radius*: According to Section III. C, the beam spot radius can be used to depict the beam distribution. We set focal length $f_R = 880$ mm and radius parameter $b_g = 1.5$ mm for the lens-like gain module D_0 [16]. The reflector M1 is a curved mirror and its curvature radius $\rho_1 = -880$ mm, which can be used to compensate for the lens-like effect of D_0 . The M1 and D_0 are set adjacent considering the integration of elements in the transmitter. The curvature radius of M2 is 10 m. $f_1 = 10$ mm, and $f_2 = f_1 M$, which expresses the focal length of D_1 , D_2 , respectively. The TIM's parameter $M = 3.5$. The distance between TIM and the left side of the gain module is 100 mm, considering the geometric length of the elements. Taking

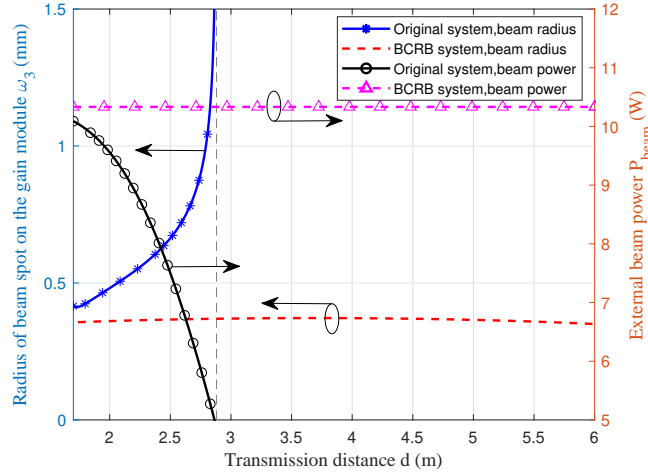


Fig. 8. Beam spot radius on gain module and beam power versus transmission distance

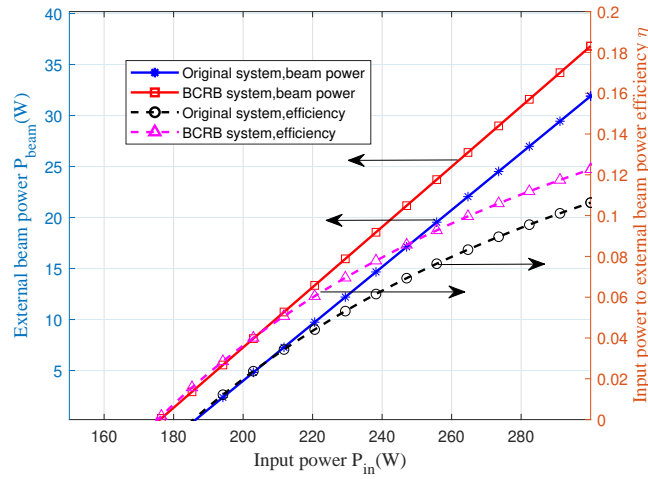


Fig. 9. Beam power and input energy to beam power efficiency versus input power

these parameters into (4), (8) and (9), the relationship of the spot radius on the gain module ω_3 and transmission distance d is given in Fig. 8. As can be seen, the beam spot radius of the BCRB system with the TIM can keep less than 0.4 mm, while the original system's beam spot radius without TIM is more than 0.4 mm. Moreover, as the transmission distance increases, the beam spot radius of BCRB changes smoothly, while the beam spot radius of the original system drastically increases to 1.5 mm. These results prove that the BCRB system can effectively compress the incident beam, and the compression state can be maintained in different ranges.

2) *Transmission performance*: We set the effective reflectivity $R = 0.2618$, the constant $C = -51.83$, the energy stored in the gain module $P_{in} = 210$ W, and the compounded energy conversion efficiency $\eta_c = 0.3384$ [16]. The geometric radius of the gain module and TIM are 1.5 mm and 10 mm, respectively. Taking parameters above into (10), the relationship between the external beam power P_{beam} and the transmission distance d of the system can be depicted. In Figure 8, the external beam power of the BCRB system with TIM can remain at 10.3 W with the increase of the transmission distance from 1.5 to 6 m, which proves the diffraction loss is effectively reduced through the beam compression. In contrast, P_{beam} of the original decreases nearly 50% to 5 W at $d = 3$ m which presents a high power attenuation. In general, the BCRB system outperforms the original in output power and transmission distance.

3) *External beam power*: We take $d = 2.6$ m as a reference point [16]. Then, substituting the above boundary parameters into (10), the relationship of external beam power, energy efficiency, and input power can be presented in Fig. 9. As is shown in straight lines, beam power of systems both linearly increases with the P_{in} charging from 150 W to 300 W. However, two systems have differences in threshold power and slope efficiency, where BCRB has lower threshold power and higher slope efficiency presenting a better power performance. Moreover, the input power to the beam power efficiency of systems presents a non-linear trend of increase with the P_{in} increasing. When P_{in} is 300 W, the conversion efficiency of the BCRB system can be 0.12 while the original system is 0.1. According to Fig. 8 and the analysis model in Section III, the transmission loss is inhibited in the BCRB system due to its beam-compression capability, and less power loss makes the system can operate in lower input power.

In summary, compared with the original system, the BCRB system can achieve effective and steady beam-compression, which makes the system has high power output over a longer distance. Overall, BCRB shows an enhanced transmission performance.

B. Achievable Performance of BCRB System

According to the analysis above, the transmission performance of the BCRB system is superior to the original system. In this part, through analyzing the stable condition, the beam spot radius, the output power, and the spectral efficiency, we will further evaluate the achievable performance of the BCRB system.

1) *Stable transmission distance*: Stable condition is the prerequisite for system operation, which ensures the beam oscillation between the receiver and the transmitter. We can get the

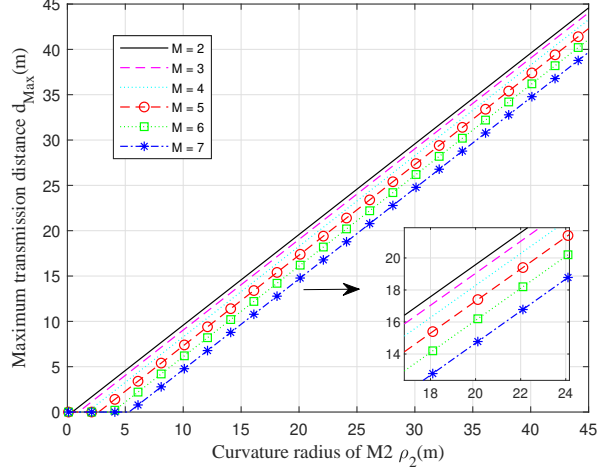


Fig. 10. Maximum transmission distance versus curvature radius of M2

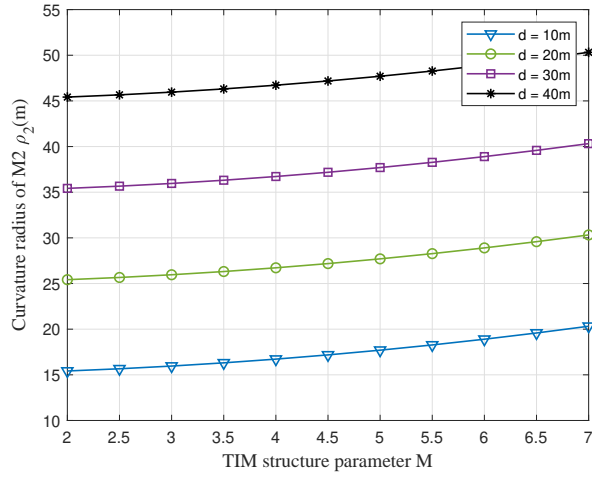


Fig. 11. Curvature radius of M2 versus TIM structure parameter

maximum stable transmission distance through the inequality of stable conditions. It is worth noting that due to the existence of the TIM, the transmission loss is suppressed, and the distance obtained from the stable inequality can be considered as the maximum transmission distance of the system. Based on the theoretical model in Section III, considering some parameters are constant and have no direct impact on the stable condition, we mainly evaluate the impact of M and ρ_2 on the BCRB system.

Taking the constant parameters determined in Section IV, part A into (4) and (7), the relation-

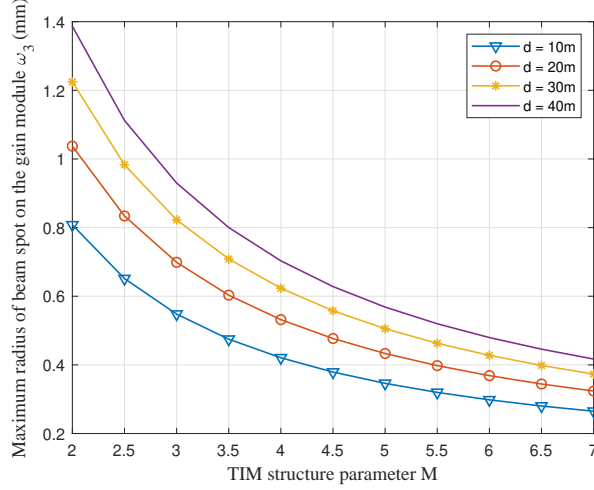


Fig. 12. Maximum beam spot radius on the gain module versus TIM structure parameter

ship between curvature radius ρ_2 and the theoretical maximum transmission distance d_{Max} of the system is depicted in Fig. 10. The values of d_{Max} increase linearly as ρ_2 increases. According to the principles of optics, the beam will diverge with the increase of the transmission distance and its curvature of the wavefront will be increased. Thus, the reflective surface of reflector M2 is supposed to have a large curvature to support effective beam reflecting. Moreover, when the value of parameter ρ_2 is fixed, d_{Max} decreases with the increase of M . The curves move downward as M increases, generally. From the analysis model in Section III, the parameter $M = f_2/f_1$, and f_1, f_2 are characteristic parameters of TIM which determine the optical capability of the lenses. Thus, the change of M will impact the system.

To further analyze the impact of M and ρ_2 on the system, we set $d = 10, 20, 30, 40$ m as evaluation points and obtained the relationship of them, which is depicted in Fig. 11. The values of ρ_2 slowly rise as M increases. When the value of M is fixed and d takes a large value, to ensure the stable condition, ρ_2 needs to match a large value. From the above evaluation results, when the BCRB system needs to operate in long-distance, to meet the stable condition, ρ_2 should take a large value. Furthermore, the value of M will also affect the transmission range, but the influence is slight, relatively.

2) *Beam spot radius*: In Part A, through comparison, the BCRB system presents a stable compression capability for incident beam. To obtain the compression limit and influencing factors, we conduct further analysis. Since the beam spot radius will be different at different

distances, we use the maximum value of the spot radius $\omega_{3,Max}$ on the gain module to analyze. We still set $d = 10, 20, 30, 40$ m as evaluation point. Based on (4), (8), (9), Table I, Table II, and the parameters determined above, the relationship curves between $\omega_{3,Max}$ and M can be obtained. In Fig. 12, the curves present a sharp downtrend at first, and then the decline becomes smooth gradually. Furthermore, when d takes a constant value, the maximum beam spot radius $\omega_{3,Max}$ will decrease with the increase of M , and if M is fixed, $\omega_{3,Max}$ will increase with the d gaining. Overall, M can affect the compression capability, a large value of M leads to greater beam compression. However, the incident beam can not achieve unlimited compression through changing M , since other parameters such as ρ_1 and L_1 will also affect the beam compression. In general, we can strengthen the compression capability by adjusting the parameter M in a certain range.

3) *Energy output*: Through the function of the beam splitter, one part of the external beam will be delivered into the PV cells for power supply, the rest will be detected by APD for data receiving. To evaluate the performance of the power output, we set the $\mu = 1$ which means the system is only used for charging at this time. Then, we take the parameters of the PV cell $a_1 = 0.3487$, and $b_1 = -1.535$ [16]. Substituting these parameters into (10) and setting the different boundary parameters P_{in} , the relationship between the output power P_{out} and transmission distance d can be obtained. As shown in Fig. 13, with the increase of transmission distance, the values of P_{out} will maintain a certain value in a long-range. Then, the curve of P_{out} presents a downtrend after passing through the critical point and will reduce to 0 W, finally. When P_{in} takes a small value, the entire curves of P_{out} move down, and the range of the transmission distance constricts slightly. In numerical level, P_{out} can be 6 W when the value of P_{in} takes 250 W, and the stable power output range can nearly reach to 200 m.

4) *Data receiving*: The proposed system can effectively enhance the transmission performance, which will also benefit the data receiving. We take optical-to-electrical conversion responsivity of APD $\gamma = 0.6$ A/W [33], the bandwidth of the noise $B_x = 811.7$ MHz [34], the electron charge $q = 1.6 \times 10^{-6}$, the background current $I_{bg} = 5100 \mu A$ [35], the boltzmann constant $K = 1.38 \times 10^{-23}$, the background temperature $T = 300$ K, and load resistor $R_L = 10 K\Omega$ [31]. We set the input power $P_{in} = 200$ W as a reference point, and take split ratio $\mu = 0.01, 0.1, 0.5, 0.9$ and 0.99 . According to these boundary parameters, (10), and (13)-(14), the relationship between the spectral efficiency \tilde{C} and transmission distance d with different split ratio μ can be obtained in Fig. 14. As is shown, when the μ is fixed, the curves present a trend of smooth changes firstly

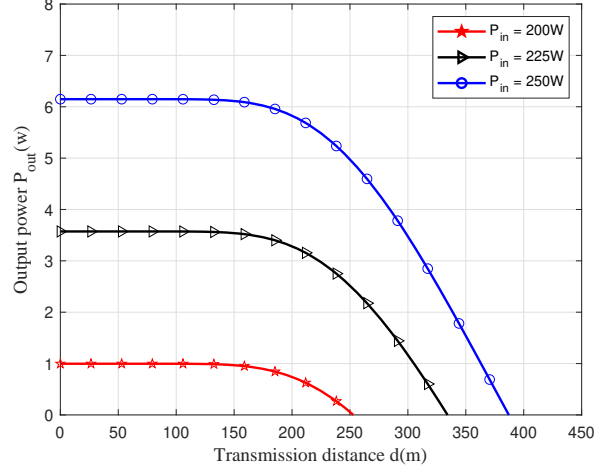


Fig. 13. Output power versus transmission distance

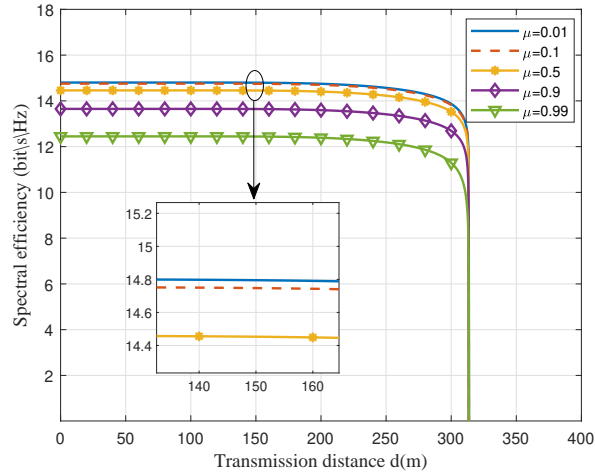


Fig. 14. Spectral efficiency versus transmission distance d with different split ratio

and then decreases sharply. The spectral efficiency can maintain a certain value in a large range of distance, which proves the system's stability. What's more, when the value of μ decreases, the spectral efficiency increases, and curves move up overall. In numerical level, when the $P_{in} = 200$ W, the spectral efficiency changes from 12.5 - 14.8 bit/s/Hz with different value of μ . To further explore the impact of input power on spectral efficiency, we set the split $\mu = 0.9$ as a reference point, and take input power $P_{in} = 200, 225$ and 250 W. After the parameters substitution and formula calculation, the relationship between the spectral efficiency \tilde{C} and transmission distance

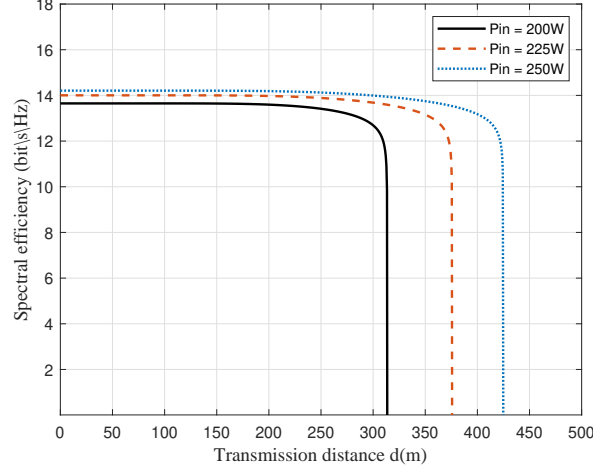


Fig. 15. Spectral efficiency versus transmission distance with different input power

d with different input power P_{in} can be obtained in Fig. 15. As can be seen, with the increase of the P_{in} , the BCRB system can have a large value of spectral efficiency \tilde{C} and a longer range of the transmission distance, which proves that high input power benefits the improvement of the transmission range and the spectral efficiency.

In general, the calculation results above show that the BCRB has the capability to supply stable high power output and data receiving over long distances.

V. CONCLUSIONS

To enhance the transmission performance of the resonant beam SWIPT systems, a beam-compress resonant beam (BCRB) design is proposed in this paper. Based on the telescope-like internal modulator (TIM), the divergence of the resonant beam is compressed and the transmission loss is restrained, which leads to the long-range transmission for the optical wireless information and power transfer. An analytical model of the BCRB system is developed to evaluate transmission stability, transmission loss, output power, and spectral efficiency. Numerical results illustrate that the proposed BCRB system can transfer 6 W power and enable 14 bit/s/Hz spectral efficiencies over 200 m, which significantly outperforms the existing RB systems.

There are some interesting topics worthy of further study in the future: 1) the battery charging performance optimization of the BCRB system, 2) the influence of the air on beam transfer in different outdoor scenarios.

Specifically, for topic 1, a feedback module can be added to the BCRB system, which realizes dynamically powering the battery. For topic 2, the impact of extreme weather on the resonant beam can be analyzed, such as dust and rainstorm.

REFERENCES

- [1] R. Zhang and C. K. Ho, "MIMO broadcasting for simultaneous wireless information and power transfer," *IEEE Transactions on Wireless Communications*, vol. 12, no. 5, pp. 1989–2001, Mar. 2013.
- [2] K. Georgiou, S. Xavier-de Souza, and K. Eder, "The IoT energy challenge: A software perspective," *IEEE Embedded Systems Letters*, vol. 10, no. 3, pp. 53–56, Jun. 2017.
- [3] K. David and H. Berndt, "6G Vision and Requirements: Is There Any Need for Beyond 5G?" *IEEE Vehicular Technology Magazine*, vol. 13, no. 3, pp. 72–80, July. 2018.
- [4] M. S. Bahbahani and E. Alsusa, "A cooperative clustering protocol with duty cycling for energy harvesting enabled wireless sensor networks," *IEEE Transactions on Wireless Communications*, vol. 17, no. 1, pp. 101–111, Jan. 2018.
- [5] K. Wang, Y. Wang, Y. Sun, S. Guo, and J. Wu, "Green industrial internet of things architecture: An energy-efficient perspective," *IEEE Communications Magazine*, vol. 54, no. 12, pp. 48–54, Dec. 2016.
- [6] K. Huang and E. Larsson, "Simultaneous information and power transfer for broadband wireless systems," *IEEE Transactions on Signal Processing*, vol. 61, no. 23, pp. 5972–5986, 2013.
- [7] N. Shinohara, *Wireless power transfer via radiowaves*. Wiley Online Library, 2014.
- [8] H. Haken, "Laser theory," in *Light and Matter Ic/Licht und Materie Ic*. Springer, 1970, pp. 1–304.
- [9] S. Das, A. Sparks, E. Poves, S. Videv, J. Fakidis, and H. Haas, "Effect of sunlight on photovoltaics as optical wireless communication receivers," *Journal of Lightwave Technology*, pp. 1–1, 2021.
- [10] Q. Liu, J. Wu, P. Xia, S. Zhao, W. Chen, Y. Yang, and L. Hanzo, "Charging unplugged: Will distributed laser charging for mobile wireless power transfer work?" *IEEE Vehicular Technology Magazine*, vol. 11, no. 4, pp. 36–45, 2016.
- [11] M. Liu, H. Deng, Q. Liu, J. Zhou, M. Xiong, L. Yang, and G. B. Giannakis, "Simultaneous mobile information and power transfer by resonant beam," *IEEE Transactions on Signal Processing*, pp. 1–1, 2021.
- [12] M. A. Khalighi and M. Uysal, "Survey on free space optical communication: A communication theory perspective," *IEEE communications surveys & tutorials*, vol. 16, no. 4, pp. 2231–2258, 2014.
- [13] W. Chen, S. Zhao, Q. Shi, and R. Zhang, "Resonant beam charging-powered UAV-assisted sensing data collection," *IEEE Transactions on Vehicular Technology*, pp. 1–1, Oct. 2019.
- [14] Q. Zhang, W. Fang, Q. Liu, J. Wu, P. Xia, and L. Yang, "Distributed laser charging: A wireless power transfer approach," *IEEE Internet of Things Journal*, vol. 5, no. 5, pp. 3853–3864, Oct. 2018.
- [15] Q. Zhang, W. Fang, M. Xiong, Q. Liu, J. Wu, and P. Xia, "Adaptive resonant beam charging for intelligent wireless power transfer," *IEEE Internet of Things Journal*, vol. 6, no. 1, pp. 1160–1172, 2018.
- [16] W. Wang, Q. Zhang, H. Lin, M. Liu, X. Liang, and Q. Liu, "Wireless energy transmission channel modeling in resonant beam charging for IoT devices," *IEEE Internet of Things Journal*, vol. 6, no. 2, pp. 3976–3986, Apr. 2019.
- [17] M. Xiong, Q. Liu, M. Liu, X. Wang, and H. Deng, "Resonant beam communications with photovoltaic receiver for optical data and power transfer," *IEEE Transactions on Communications*, vol. 68, no. 5, pp. 3033–3041, Feb. 2020.
- [18] M. Xiong, M. Liu, Q. Zhang, Q. Liu, J. Wu, and P. Xia, "TDMA in adaptive resonant beam charging for IoT devices," *IEEE Internet of Things Journal*, vol. 6, no. 1, pp. 867–877, Feb. 2019.
- [19] W. Fang, Q. Zhang, Q. Liu, J. Wu, and P. Xia, "Fair scheduling in resonant beam charging for IoT devices," *IEEE Internet of Things Journal*, vol. 6, no. 1, pp. 641–653, Feb. 2019.

- [20] W. Fang, H. Deng, Q. Liu, M. Liu, Q. Jiang, L. Yang, and G. B. Giannakis, "Safety analysis of long-range and high-power wireless power transfer using resonant beam," *IEEE Transactions on Signal Processing*, 2021.
- [21] M. S. Aziz, S. Ahmad, I. Husnain, A. Hassan, and U. Saleem, "Simulation and experimental investigation of the characteristics of a pv-harvester under different conditions," in *2014 International Conference on Energy Systems and Policies (ICESP)*. IEEE, 2014, pp. 1–8.
- [22] J. C. Campbell, "Recent advances in telecommunications avalanche photodiodes," *Journal of Lightwave Technology*, vol. 25, no. 1, pp. 109–121, 2007.
- [23] A. Al-Kinani, C.-X. Wang, L. Zhou, and W. Zhang, "Optical wireless communication channel measurements and models," *IEEE Communications Surveys & Tutorials*, vol. 20, no. 3, pp. 1939–1962, 2018.
- [24] M. Eichhorn, *Laser physics: from principles to practical work in the lab*. Springer Science & Business Media, 2014.
- [25] W. Koechner, *Solid-state laser engineering*. Springer, 2013, vol. 1.
- [26] R. N. N. Hodgson and I. H. Weber, *Laser Resonators and Beam Propagation*. Springer, 2005, vol. 108.
- [27] M. Born and E. Wolf, *Principles of optics: electromagnetic theory of propagation, interference and diffraction of light*. Elsevier, 2013.
- [28] H. Kogelnik, "Imaging of optical modes—resonators with internal lenses," *Bell System Technical Journal*, vol. 44, no. 3, pp. 455–494, Mar. 1965.
- [29] H. Kogelnik and T. Li, "Laser beams and resonators," *Appl. Opt.*, vol. 5, no. 10, pp. 1550–1567, Oct. 1966.
- [30] P. Baues, "Huygens' principle in inhomogeneous, isotropic media and a general integral equation applicable to optical resonators," *Opto-electronics*, vol. 1, no. 1, pp. 37–44, Feb. 1969.
- [31] F. Xu, M. Khalighi, and S. Bourennane, "Impact of different noise sources on the performance of pin- and apd-based fso receivers," in *Proceedings of the 11th International Conference on Telecommunications*, Jun. 2011, pp. 211–218.
- [32] A. Lapidith, S. M. Moser, and M. A. Wigger, "On the capacity of free-space optical intensity channels," *IEEE Transactions on Information Theory*, vol. 55, no. 10, pp. 4449–4461, 2009.
- [33] M. S. Demir, F. Miramirkhani, and M. Uysal, "Handover in vlc networks with coordinated multipoint transmission," in *2017 IEEE International Black Sea Conference on Communications and Networking (BlackSeaCom)*, Jun. 2017, pp. 1–5.
- [34] C. Quintana, Q. Wang, D. Jakonis, X. Piao, G. Erry, D. Platt, Y. Thueux, A. Gomez, G. Faulkner, H. Chun, M. Salter, and D. O'Brien, "High speed electro-absorption modulator for long range retroreflective free space optics," *IEEE Photonics Technology Letters*, vol. 29, no. 9, pp. 707–710, Mar. 2017.
- [35] A. J. Moreira, R. T. Valadas, and A. de Oliveira Duarte, "Optical interference produced by artificial light," *Wireless Networks*, vol. 3, no. 2, pp. 131–140, May. 1997.